

# **EXPERIMENTAL INVESTIGATIONS OF THE AERODYNAMICS OF AN ANNULAR COMPRESSOR CASCADE AT REVERSED FLOW CONDITIONS**

*V.Chenaux<sup>1</sup> - H.Schönenborn<sup>2</sup> - P.Ott<sup>1</sup>*

<sup>1</sup>Laboratoire de Thermique Appliquée et de Turbomachines, Ecole Polytechnique Fédérale de Lausanne, Lausanne, Switzerland. Email: [virginie.chenaux@epfl.ch](mailto:virginie.chenaux@epfl.ch), [peter.ott@epfl.ch](mailto:peter.ott@epfl.ch)

<sup>2</sup>MTU Aero Engines GmbH, München, Germany. Email: [harald.schoenenborn@mtu.de](mailto:harald.schoenenborn@mtu.de)

## **ABSTRACT**

**Compressor unsafe operating regimes yield unsteady high speed turbulent flows in which complex aeroelastic phenomena occur. If the blade flutter and forced response behavior (i.e. aeroelastic stability) can be predicted reliably for normal flow conditions, its assessment at severe-off design conditions remains a critical task for compressor development programs. Due to complex flow fields and highly transient phenomena, reversed flow conditions are still difficult to predict. Within this frame, the understanding of the physical mechanisms of surge onset and events is essential to improve surge occurrence prediction and control.**

**This paper presents steady-state results of an experimental investigation performed on an annular compressor cascade subjected to constant subsonic backflow inlet conditions. The investigations were carried out at EPF Lausanne, in the annular test facility for non-rotating cascades. With an upstream swirled flow corresponding to real axial turbomachine conditions, an axisymmetric flow can be achieved in the test section.**

**This paper constitutes an introduction and a basis to an associated forthcoming experimental study, dedicated to aeroelastic investigations.**

**The steady-state flow conditions are measured upstream and downstream of the test section, with 5-hole aerodynamic probes. The compressor cascade consists of 20 blades, mounted on 20 independent elastic springs and masses to enable the excitation of different IBPA during the aeroelastic measurements. A pair of blades was instrumented with respectively pressure and suction side pressure taps along the airfoil chord length in order to measure the surface steady-state pressure. Static pressure taps were also inserted in the casing of the test section to assess flow characteristics in the blade tip area.**

**To provide a comparison tool to the measurements, associated CFD calculations at off-design conditions were performed. The comparison between CFD and measurements shows a high level of confidence. Since not many experiments exist at severe off-design conditions, these experimental results are a precious data source for CFD validation.**

## **NOMENCLATURE**

### **Variables**

$c$	blade chord
$c_{ax}$	blade axial chord
$M$	Mach number
$p$	pressure
$\beta$	relative flow angle
$T$	temperature
$c_p$	turbine pressure coefficient
$C_p$	compressor pressure coefficient
$r$	normalized radial direction
$H$	channel height
$\varphi$	circumferential direction

## **Subscripts**

t	total quantity
1	upstream flow conditions
2	downstream flow conditions
av	average value

## **Abbreviations**

LE	leading edge
TE	trailing edge
PS	pressure side
SS	suction side
US	upstream test section
DS	downstream test section

## **INTRODUCTION**

The demands for high performance, light and compact engines result in higher aerodynamic loading and lower blade stiffness trends. To improve compressor effectiveness and efficiency, the engine is subjected to higher pressure ratios and higher flow velocities around the blades. This requires the extension of the compressor stable operating range and thus, an accurate prediction of the blade loading during the design phase.

In the compressor system, higher performance is often associated with extension of the engine operating flow range. Within this frame, high operating pressure levels combined with high speeds are the solution, but such conditions can also endanger the compressor flow regimes stability, inducing unsteady flows and complex aeroelastic phenomena. As a consequence of these flow instabilities, off-design flow conditions arise and affect the dynamic structural behavior as well as the aeroelastic stability of the blades. Due to large pressure fluctuations, surge events (reversed flow conditions) excite high-amplitude flow-induced vibrations and can damage the compression system. Because of complex flow fields and highly transient phenomena, the predictions of reversed-flow conditions during the design phase remain complicated.

An important part of the compressor research is therefore, first, the better understanding of the physical mechanisms of surge onset and events and second, the prediction and control of surge occurrence in order to extend the operating range of engines. Within the last years, significant progress has been documented in this field, with both aerodynamics and aeroelastic approaches.

Investigations were carried out in order to understand surge phenomenon. Day, [2] and [3]. Gamache and Greitzer [10] did some extensive experimental work to investigate the 3D-flow field structures during reversed flow conditions. Fleeter [9] investigated experimentally the unsteady fluid-dynamic excitations of compressor flow instabilities, their vibration levels and their impact on the blades. Several numerical models were developed in order to control and overcome surge: Greitzer and Moore [1] investigated the system stability and developed a simplified model able to predict surge and rotating stall for low speed axial engines. This study was validated with experimental data. Mazzawy [6] developed a model to estimate surge loads in the entire compressor system.

With the improvement of computational performance, models of compressor system surge progressively appear (Niazi, [4] and Vahdati [5]). Di Mare [17] carried out flutter stability computations for various severe off-design conditions and various mode shapes, and noted that aerodynamic damping in surge flow conditions is reduced compared to normal flow conditions. Rudy [7] and Schöenborn [8] adopt a combined approach of both aerodynamic and mechanical effects of surge.

Experimental investigations on turbine cascades were carried out by Körbächer [15] and Cinnella et al.[18]. Operating the cascade at off-design flow conditions revealed a separation bubble on the blade SS, and a stagnation point on the blade PS. Carstens et al. [16] compared experimental and numerical data: a transonic turbine cascade was subjected to both normal and off-design flow

conditions. Numerical simulations showed the difficulties of Euler codes to capture the flow characteristics present at the blade SS.

Only few experimental data exist at severe off-design conditions. Especially at reversed flow conditions (surge blow-down phase), data is needed by the aeroelastic research community to validate dedicated models and numerical codes. This paper presents the experimental steady-state results of a compressor cascade test model operated at constant backflow conditions. The measurements are carried out for different inlet Mach numbers and inflow incidences and include blade surface pressures, downstream flow fields and casing wall pressures. Numerical calculations results associated to the experimental test cases are included in the second part of the paper, to provide a comparison tool between both approaches.

## EXPERIMENTAL SETUP

The experimental investigations presented here were performed in the Non-Rotating Annular Test Facility at EPFL (Bölcs, [11]). This test rig enables the study of steady-state and unsteady flows in both turbine and compressor annular cascades without having to rotate them. A radial-axial nozzle combined with pre-swirl vanes generates a spiral flow corresponding to the relative flow in axial turbomachines. Sub-, trans- or supersonic flow conditions can be achieved in the test section. The advantage of avoiding the rotation is to enable extensive test model instrumentation on compressor or turbine rows, combined with low data acquisition and data transfer requirements.

A schematic view of the annular facility is presented in Figure 1 (A). The test rig is supplied with a 2.25 MW centrifugal compressor. The air exiting the compressor is cooled by two heat exchangers, in order to regulate the air temperature in the test section, within a range of 10°C and 60°C. Air enters the test rig through two independent inlet valves and is turned through a pair of pre-swirl vanes. These vanes enable the adjustment of the inlet flow conditions over the channel height. The adjustment consists in achieving a quasi two-dimensional flow at mid-channel height. The inlet flow conditions can be adjusted with three parameters: total pressure, outlet pressure and inlet flow angle.

The compressor cascade is composed of 20 prismatic blades. A special configuration consisting in flipping the airfoil was adopted in order to satisfy the backflow inlet conditions required for the study. A scheme of the test model configuration is included in Figure 1 (B). Basic airfoil characteristics are included in Figure 1 (C). Two blades were equipped with pressure taps in order to measure the steady-state surface static pressure. The pressure taps are located at mid-channel height (50% of the blade span), and constitute a pair of PS and SS measuring blades. An overview of the measuring setup is depicted Figure 1 (D). The distribution of the blade surface measuring locations is presented in Figure 1 (E). The tip clearance over 360° is included within a range of 0.6% and 1.8% span. Note that the compressor cascade complexity is due to aeroelastic investigations perspectives.

Steady-state flow conditions are measured by aerodynamic 5-hole probes, upstream and downstream of the test section. After a calibration process, the pressures measured by the probes enable the determination of total pressures  $pt_1$  and  $pt_2$ , steady pressures  $p_1$  and  $p_2$ , as well as the interpolation of Mach numbers  $Ma_1$ ,  $Ma_2$  and flow angles  $\beta_1$  and  $\beta_2$ . Two-step motor driven probe-holders, combined with a step indexing feature allow the flow mapping over the radial and circumferential directions. Typically, 15 radial positions are measured over 18°, in steps of 1°, which corresponds to one inter-blade passage. 18 axial measuring locations are included in the casing, Figure 1 (E), to provide flow field data in the blade tip area (18 axial position measured over one blade passage). For a detailed description of the measuring techniques and measurement accuracy, see reference [19].

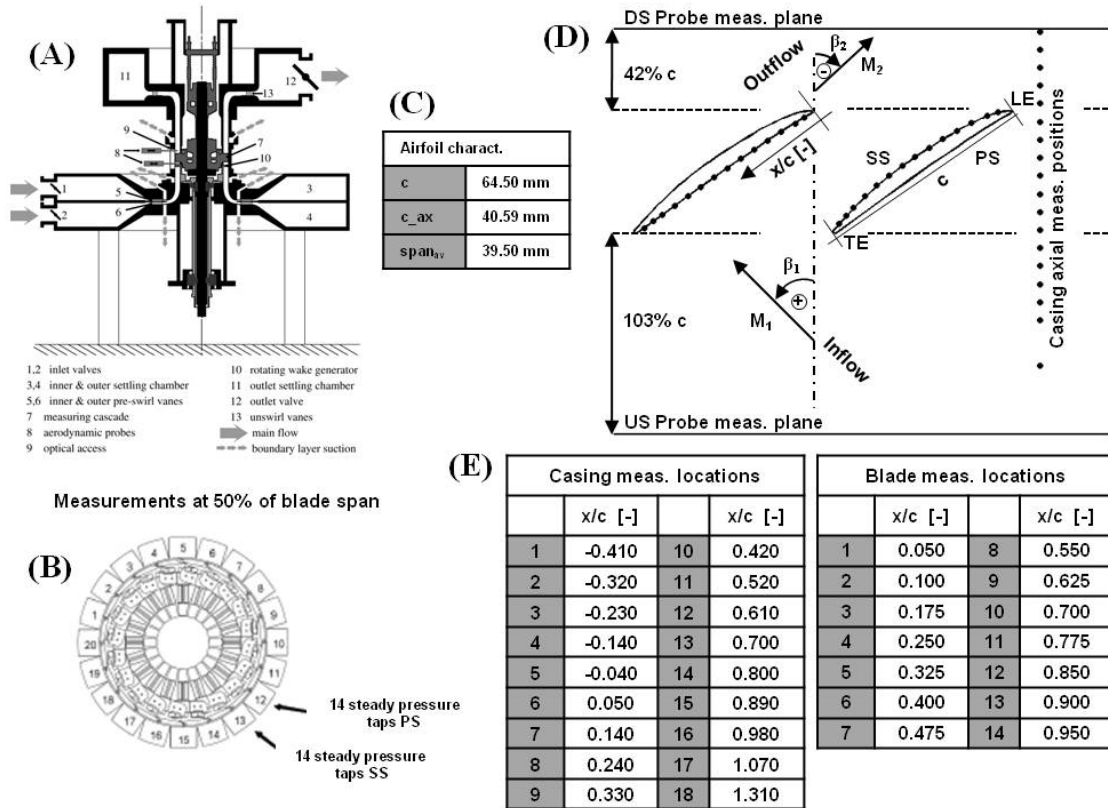


**Figure 1: (A) EPFL Non-Rotating Annular Test Facility. (B) Cascade instrumentation (view from downstream side). (C) Basic specifications of compressor airfoil. (D) 2D measuring setup (view towards hub), with casing and probes axial measuring locations, and PS/SS blade surface pressure taps locations. The flow enters the test section at the blade TE and leaves the passage at the LE. (E) Steady-state blade surface and axial casing measuring locations with respect to  $x/c$  [-] 1D coordinate system.**

## EXPERIMENTAL DATA

### Investigated flow cases

In order to compare the influence of the inlet flow angle and Mach number on the blade surface pressures and DS flow fields, five operating points were investigated. Three Mach number levels were tested, ranging from  $M_1=0.2$  to  $M_1=0.5$ . The inflow incidence was varied from  $\beta_1=45^\circ$  up to  $\beta_1=71^\circ$ . It constitutes the widest operation field achievable in the test rig with the present compressor cascade. The measured probe pressures  $pt_1$ ,  $pt_2$ ,  $p_1$  and  $p_2$  were used to compute mass flow averaged flow parameters, up- and downstream of the test section. The investigated flow cases are listed in Table 1. Note that due to the reversed-flow conditions, the flow is accelerated through the compressor inter-blade passage, which may be associated to typical turbine flow conditions. Due to the combination of high incidence angle and low inlet Mach number, test case  $0.2/71^\circ$  experiences low Mach number acceleration through the passage.

Inlet flow parameters	Low Mach number test cases						High Mach number test cases			
	0.2/45°		0.2/55°		0.2/71°		0.5/71°		0.4/50°	
Axial position	US	DS	US	DS	US	DS	US	DS	US	DS
Mach number $M$ [-]	0.20	0.37	0.20	0.34	0.20	0.21	0.49	0.57	0.38	0.85
Rel. flow angle $\beta$ [°]	44.91	-60.90	54.89	-63.77	71.27	-69.67	69.56	-64.23	49.85	-56.3

**Table 1. Steady-state mass flow averaged flow conditions, upstream and downstream of the test section**

# RESULTS AND ANALYSIS

## Steady-state surface pressure distribution

The steady-state pressures measured on the blades at 50% of the blade span were transformed to steady pressure coefficients, defined as follows:

$$c_p = \frac{p_{t1} - p}{p_{t2} - p_2} \quad (1)$$

Definition (1) corresponds to a typical turbine  $c_p$ . This representation was selected due to the reversed-flow conditions occurring in the compressor cascade; the incoming flow is accelerated through the blade passage, and thus, is representative of a turbine flow.

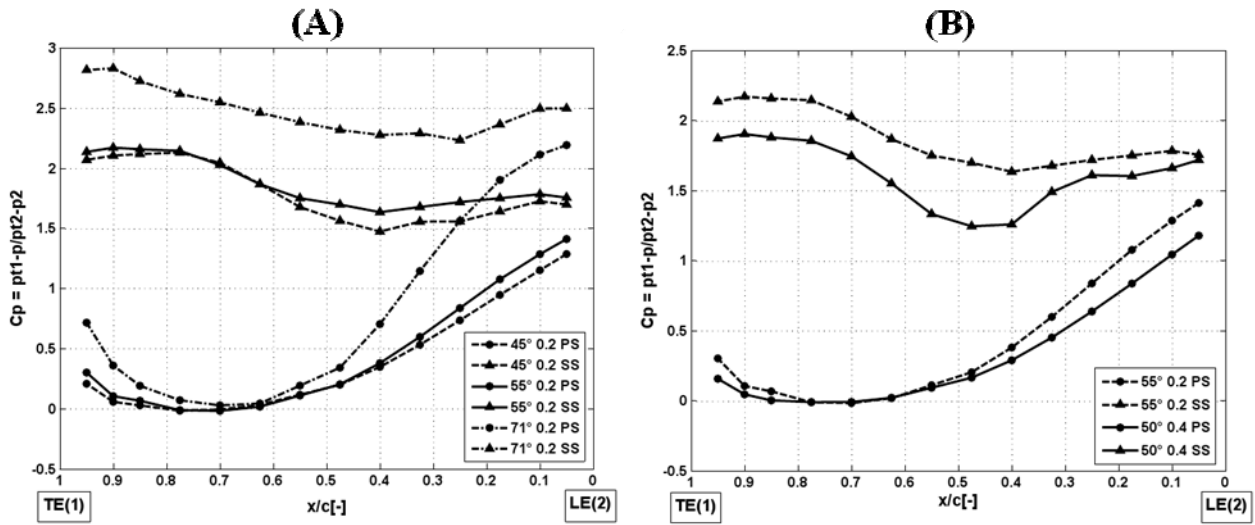


**Figure 2. (A): Blade surface pressure coefficient distribution at 50% r/H for Mach number  $M_1=0.2$  and different inlet flow angles. (B): Blade surface pressure coefficient distribution at 50% r/H for inlet flow angle  $50^\circ/55^\circ$  and different inlet Mach numbers**

Figure 2 (A) presents the pressure coefficients for three incidence angles, at constant Mach number ( $M_1=0.2$ ). Data is plotted against the normalized blade chord length, with blade trailing edge located at the origin (with respect to Figure 1, (D)). The measurement error is estimated to be in the order of the symbol thickness. The pressure coefficients for  $\beta_1=45^\circ$  and  $\beta_1=55^\circ$  present the same evolution along the blade chord, for both PS and SS. The evolution is different for incidence angle  $\beta_1=71^\circ$ , due to the increase of the circumferential velocity component.

A flow deceleration occurs on the blade PS close to the TE, followed by near zero  $c_p$  values ( $x/c=0.8$  to  $0.6$ ), corresponding to a stagnation region. The stagnation point location moves to the blade LE direction when increasing the inflow incidence. The flow is reaccelerated towards the blade LE ( $x/c=0.6$  to  $0.0$ ). For higher incidence angles ( $71^\circ$ ), the stagnation region is reduced and followed by a steeper acceleration.

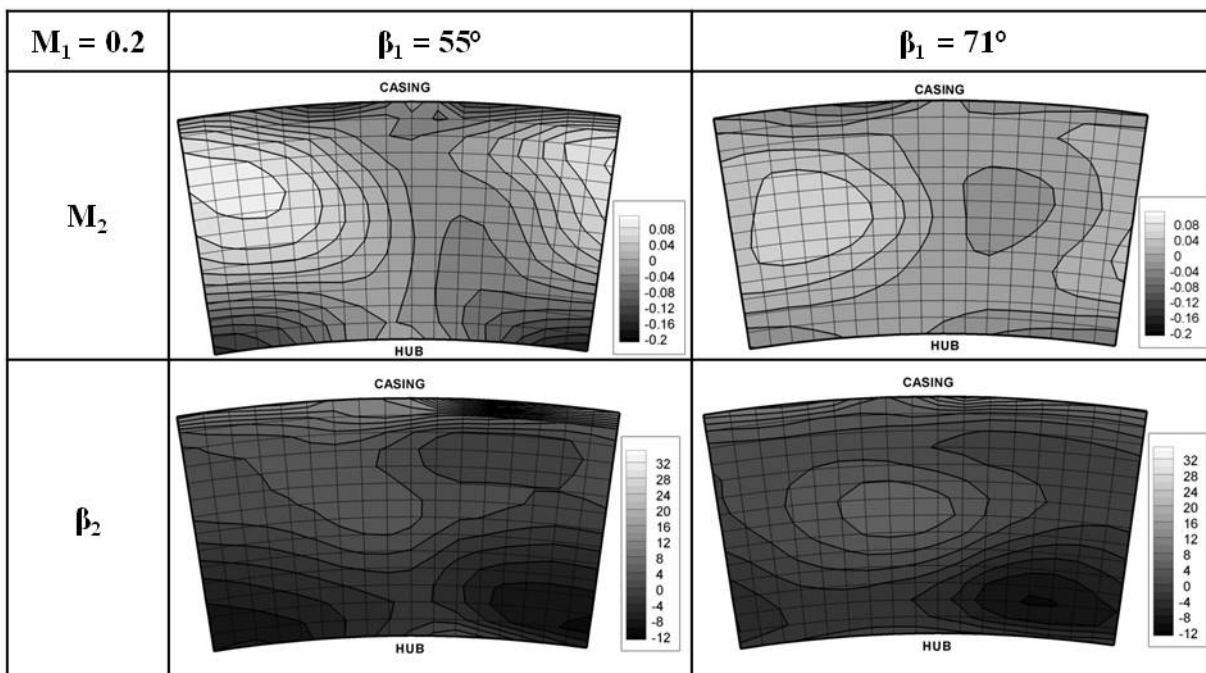
On the blade SS close to the TE, the presence of a flow separation area can be recognized by a constant  $c_p$  zone. The local pressures inside the zone are radically different from the pressure magnitudes present in the overall inter-blade passage. At this location,  $c_p$  values represent the order of magnitude of the losses generated inside the recirculation zone. After the separation zone, a deceleration occurs, due to the recirculation area. The deceleration is followed by a slight acceleration indicating flow recovery towards the blade SS LE. For the highest incidence angle, the flow separation zone is smaller but the deceleration zone is extended; the reacceleration is steeper, but occurs at  $x/c = 0.25$  blade SS, delaying the flow recovery.

Figure 2 (B) presents the pressure coefficient evolution for two inlet Mach number flow conditions. Despite the cascade was operated at non equal inlet flow angles ( $\beta_1=55^\circ$  versus  $\beta_1=50^\circ$ ),

the analysis for incidence angles between  $45^\circ$  and  $55^\circ$  revealed that the  $c_p$  curve was not modified significantly. We therefore admit that the difference between both  $c_p$  profiles depicted in Figure 2 (B) are only due to the inflow velocity changes. On the blade PS, the stagnation area is extended with increasing the Mach number. On the blade SS, local pressure losses associated to the recirculation zone are lower for high inlet flow velocities. For both test cases, the acceleration located after the recirculation zone occurs at blade  $x/c = 0.4$ , up to the blade LE. For test case  $M_1=0.4$ , the acceleration is steeper.

### Downstream steady-state flow fields

Figure 3 presents angle and Mach number spatial variation contours, downstream of the test section, over one inter-blade channel. Traverse data is plotted against the normalized channel span. The spatial variation was obtained by subtracting calculated mass flow averaged value (Table 1) from initial measured values (i.e. variation around mass flow averaged value). The cases presented are incidence angles  $\beta_1=55^\circ$  and  $\beta_1=71^\circ$  for  $M_1=0.2$ . The flow field for  $M_1=0.2$ ,  $\beta_1=45^\circ$  is similar to  $M_1=0.2$ ,  $\beta_1=55^\circ$ , and is omitted here.



**Figure 3. Spatial variations of DS flow fields measurements (outlet Mach number and outlet flow angle) for constant inlet Mach number  $M_1=0.2$  and two different inlet flow angles ( $\beta_1=55^\circ$  and  $\beta_1=71^\circ$ ). Traverse data is plotted against the normalized channel span.**

Three negative variation zones can be observed: two of them are located at the hub and casing vicinity, and can be associated to wall effects and tip leakage flow. The third negative variation cell is induced by combined effects of the blade wake and recirculation bubble. For higher incidence angles, this negative variation cell is larger in the circumferential direction, indicating an extended recirculation zone in the blade passage. For lower incidence angles, stronger velocity gradients are identified, indicating a better flow recovery. Small variations in the circumferential direction of pitch angle contours confirm this feature, whereas for higher incidence angles, two structures can still be identified.

Figure 4 depicts angle and Mach number spatial variations contours, downstream of the test section, over one inter-blade channel, for a constant inflow angle,  $\beta_1=71^\circ$ . Two inlet Mach numbers are analyzed:  $M_1=0.2$  and  $M_1=0.5$ . Traverse data is plotted against the normalized channel span.

Considering DS Mach number contours, the same flow structures can be observed on both test cases. However, outlet Mach number amplitudes and gradients are stronger for higher inlet flow

velocities. This phenomenon may be correlated with the analysis of Figure 2 (B); the stronger flow acceleration on the fore blade SS yields a better flow recovery. This is confirmed by the more uniform trend of the outlet flow angle contours in the circumferential direction.

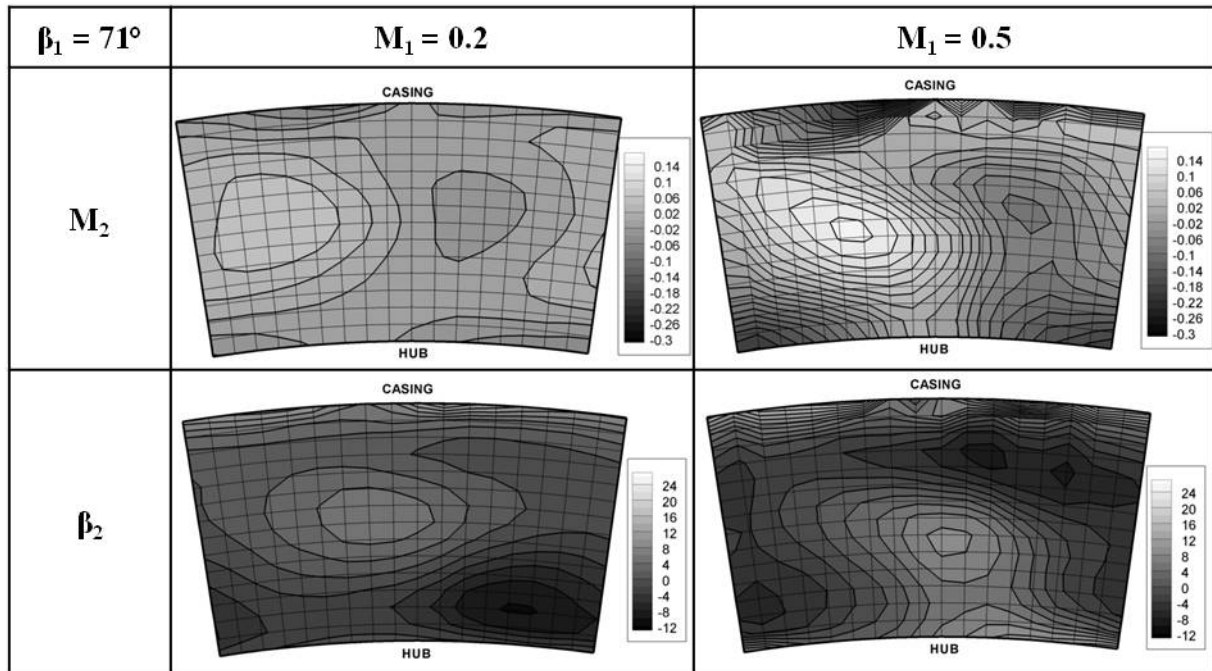


**Figure 4. Spatial variations of DS flow fields measurements (outlet Mach number and outlet flow angle) for constant inlet flow angles conditions  $\beta_1=71^\circ$  and two different inlet Mach numbers ( $M_1=0.2$  and  $M_1=0.5$ ). Traverse data is plotted over the normalized channel span.**

## COMPARISON BETWEEN EXPERIMENTAL DATA AND NUMERICAL CALCULATIONS

### Computational setup and grid

A numerical study was performed parallel to the experimental investigations. The computational setup and grid is included in Figure 5. The blade is meshed as a normal airfoil. In a second step, inlet and exit are changed, so that the metal trailing edge shows to the inlet. An O-type grid is placed directly around the blade surface and a C-type grid is created around the O-type grid. The remaining flow domain is meshed with H-type grids. A tip clearance is included based on measurements in the rig. Note that inlet and exit boundaries extent further upstream and downstream than presented in Figure 5. In previous studies, [12], it was found that the cavity flow through the slots, which are all around the airfoil, may affect the flow solution. Thus, the cavity was included into the numerical investigations and connected to the blade channel by a zonal interface, which provides an accurate connection between non-coincident grids. At the inlet, the radial total pressure profile assessed during measurements was prescribed, together with the total temperature and the inlet flow angle. At the exit, the averaged measured static pressure was fixed, assuming radial equilibrium. On the right hand side of Figure 5, the computational grid is presented. The calculations were performed with the Trace code developed at DLR [13]. In this solver, the 3-D Reynolds averaged Navier-Stokes equations are integrated in time by a fully implicit formulation of the second-order scheme for the compressible ideal or real gas in conjunction with the two equation  $k-\omega$  turbulence model, which is enhanced by some features by DLR. A more detailed description of the procedure is presented in reference [14].

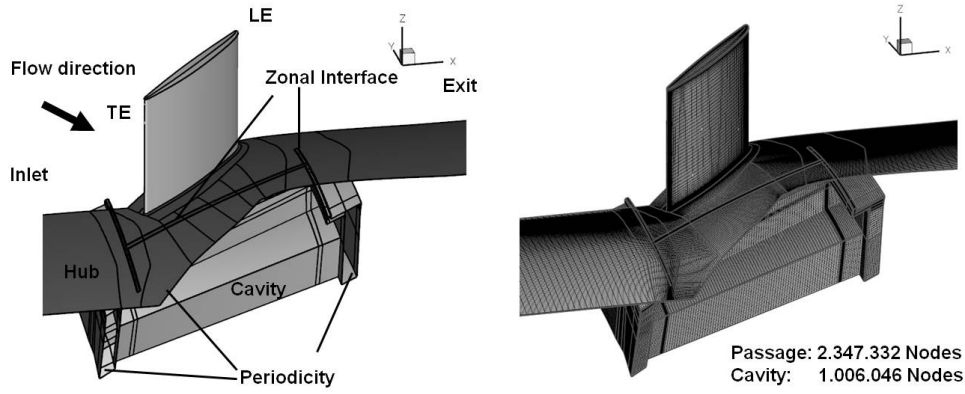
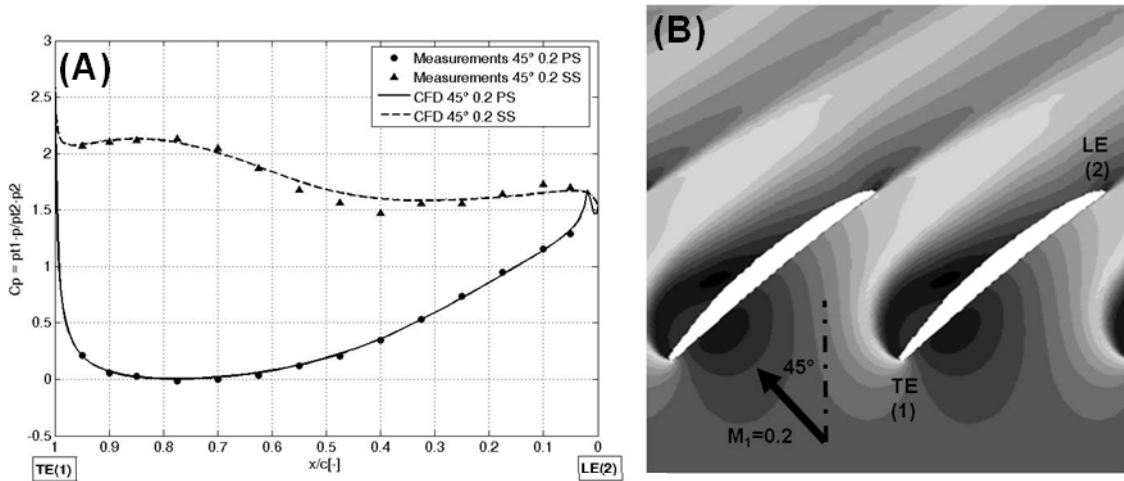


**Figure 5. Computational setup and grid (computational setup corresponds to the mirror view of the experimental cascade setup)**

## Results

The comparison is presented for flow conditions  $M_1=0.2$  and  $\beta_1=45^\circ$ . The blade steady-state surface pressure distribution obtained by measurements and numerical calculations is presented in Figure 6 (A). Whereas the agreement on the PS is perfect, SS shows slight differences in the flow recirculation zone from  $x/c = 0.65$  up to  $x/c = 0.4$ . Results for other flow cases (detailed in Table 1), are similar.

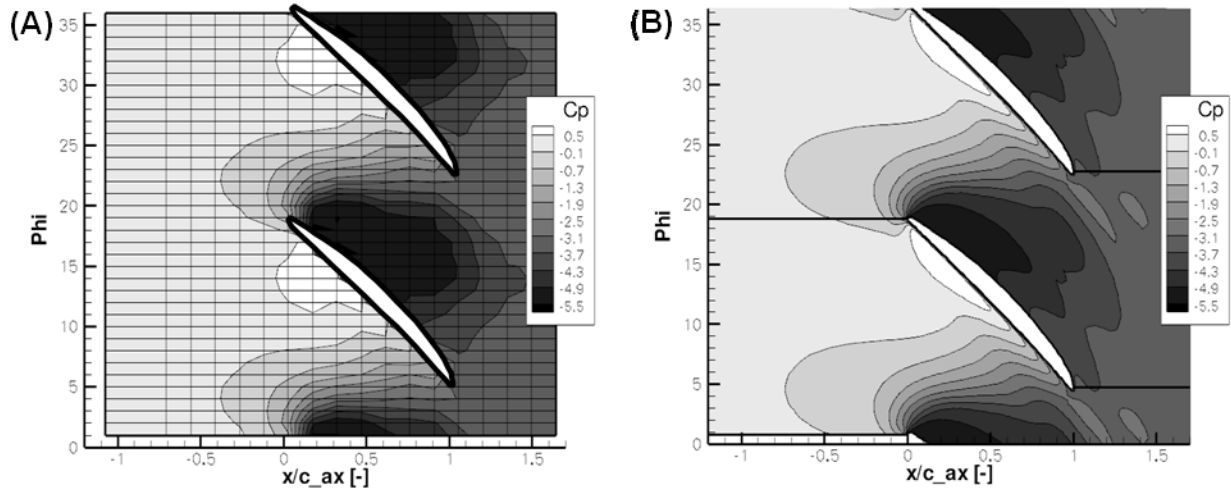
Figure 6 (B) includes the computed flow field at 50% of the channel height, where the blade surface steady-state pressures are measured. The comparison between Figure 6 and Figure 2 confirms the analysis based on the measured data. On the PS, the presence and the location of the stagnation point (stagnation area) defined on the pressure coefficient graph (Figure 2) is confirmed. On the blade SS close to the TE, a large recirculation zone can be observed, yielding flow disturbances up to outlet of the blade passage and reducing the inter-blade section.



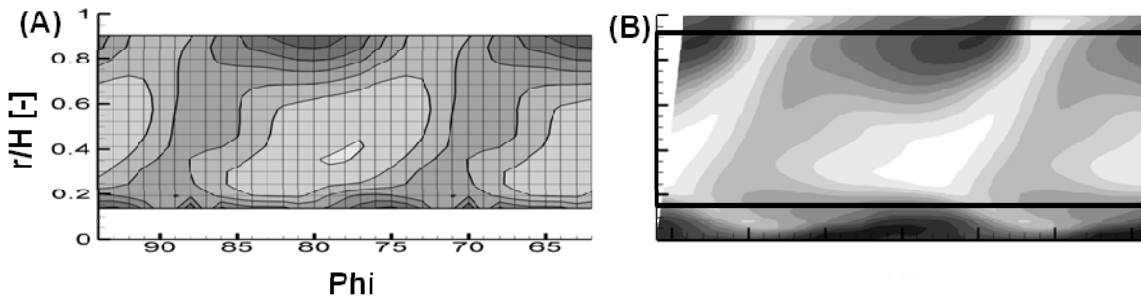
**Figure 6. (A) Blade steady-state surface pressure distribution, 50% span. Inlet flow conditions:  $M_1=0.2$ ,  $\beta_1=45^\circ$ . (B) Numerical results of the flow field at 50% of the channel height. Inlet flow conditions:  $M_1=0.2$ ,  $\beta_1=45^\circ$**

Figure 7 (A) and (B) presents casing wall pressure measurements and numerical calculations for test case  $M_1=0.2$  and  $\beta_1=45^\circ$ . To compare the results, a typical compressor pressure coefficient was selected, defined as follows:

$$C_p = \frac{p - p_1}{p_{t1} - p_1} \quad (2)$$



**Figure 7. (A) Measured casing pressure contours, (B) Calculated casing pressure contours. (View direction radially outward, inlet flow conditions:  $M_1=0.2$ ,  $\beta_1=45^\circ$ ).**



**Figure 8. (A) Measured DS Mach number contours, (B) Calculated DS Mach number contours. View from US towards DS direction, inlet flow conditions:  $M_1=0.2$ ,  $\beta_1=45^\circ$ . Same study area, same scales. Dark and light grey levels correspond to low and high Mach number, respectively.**

Contours are plotted on a plane corresponding to axial versus circumferential direction, in the radially outward direction. The numerical results match very well the measured data, and capture perfectly the complex flow field generated by the backflow inlet conditions. Figure 8 (A) and (B) compares downstream Mach number contours for test case  $M_1=0.2$  and  $\beta_1=45^\circ$ . The measured data was duplicated to provide visualization in 2 inter-blade passages. Measured radial range is included within 17.5% and 90% of channel height. Here again, the agreement between measurements and calculations results is good. Mach amplitude levels and flow structures are equivalent.

Similar results were obtained for the other flow cases. This confirms the ability of the CFD code to capture the complex flow structures present at severe off-design flow conditions.

## CONCLUSIONS

This paper presented steady-state measurements results of an annular compressor cascade subjected to constant reversed-flow conditions. Measured DS flow fields, blade surface and casing steady-state pressures were presented for various incidence angles and various inlet Mach numbers.

Blade surface measurements at 50% span detected the presence of a stagnation area on the blade PS, and a large recirculation region on the blade SS. Higher incidence angles induce higher local pressure losses in the SS recirculation zone and delay the flow recovery. A reduced stagnation area on the blade PS can be observed. Higher Mach numbers improve flow recovery after the SS recirculation zone.

For all test cases, comparisons with associated numerical calculations showed the ability of the CFD code to reproduce the complex flow field. Within this frame, this study provides a validation tool to the steady-state solution required for aeroelastic stability calculations.

From a more general standpoint, this paper constitutes a basis to future aeroelastic experimental investigations at severe off-design flow conditions (first unsteady results available in reference [14]). The unsteady experimental data will constitute a comparison and validation tool to numerical codes, in order to improve compressor aeroelastic stability predictions, during the engine design phase.

## ACKNOWLEDGEMENTS

The investigations were carried as part of a project of the MTU Aero Engines GmbH, in the frame of a German research project, Lufo IV. The authors would like to acknowledge the financial support provided and the authorization for publishing the results here. The authors extend their thanks to Dr. Kahl and Dr. Deslot for their valuable technical comments.

## REFERENCES

- [1] Greitzer, E.M., 1978, Surge and rotating stall in axial flow compressors, Part I/II, ASME Journal of Engineering for Power, 190-217
- [2] Day, I.J., 1994, Axial compressor performance during surge, Journal of Propulsion and Power, Vol.10, No.3.
- [3] Day, I.J., 1996, Stall and surge in high speed compressors and the prospects for active control. VKI LS 1996-05
- [4] Niazi, S., 2000, Numerical simulation of rotating stall and surge alleviation in axial compressors, PhD thesis, Georgia Institute of Technology, Department of aerospace engineering, USA.
- [5] Vahdati, M., Simpson, G., Imregun M., 2006, Unsteady flow and aeroelastic behavior of aero-engine core compressors during rotating stall and surge, ASME GT-90308
- [6] Mazzawy, R.S., 1980, Surge induced structural loads in gas turbines, Transactions of the ASME, 162/ Vol. 102
- [7] Rudy, M.D., 1982, Transient blade response due to surge induces structural loads, SAE Technical paper 8214338
- [8] Schöenborn, H, Breuer, T., 2004, Aerodynamic and mechanical vibration analysis of a compressor blisk at surge, Proceedings of ASME Turbo Expo, GT2004-53579
- [9] Kim, K.H., Fleeter S., Sept.-Oct. 1994, Compressor unsteady aerodynamic response to rotating stall and surge excitations, J.of Propulsion and Power, vol.10, pp.698-708,
- [10] Gamache, R. N.; Greitzer, E. M. "Reverse Flow in Multistage Axial Compressors", AIAA-paper 86-1747, AIAA/ASME/SAE/ASEE 22nd Joint Propulsion Conference, June 16-18, 1986, Huntsville, Alabama
- [11] Bölcs A., "A test facility for the investigation of steady and unsteady transonic flows in annular cascades", 1983, Proceedings of ASME, 83-GT-34.
- [12] Kahl, G.; Hennings, H.: "Computational investigation of an oscillating Compressor Cascade Experiment", 9th Symposium on unsteady Aerodynamic, Aeroacoustics and Aeroelasticity of Turbomachines ISUAAAT, 2001
- [13] Nuernberger, D., Eulitz, F., Schmitt, S., Zachcial, A.: "Recent Progress in the Numerical Simulation of Unsteady Viscous Multistage Turbomachinery Flow", ISABE-2001-1081, 2001
- [14] Schoenenborn, H., Chenaux, V., Ott, P.: "Aeroelasticity at reversed flow conditions – Part 1: Numerical and Experimental Investigations of a Compressor Cascade with Controlled Vibration", Paper GT2011-45034 submitted to the ASME TurboExpo 2011, Vancouver
- [15] Bölcs, A.; Körbächer, H.: "Periodicity and Repetivity of Unsteady Measurements of an Annular Turbine Cascade at Off-Design Flow Conditions", AMSE paper 93-GT-107, Cincinnati, Ohio, 1993

- [16] Carstens, V.; Bölcs, A.; Körbächer, H.: “Comparison of Experimental and Theoretical Results for Unsteady Transonic Cascade Flow at Design and Off-Design
- [17] Di Mare, L.d.; Krishnababu, S. K.; Mueck, B.; Imregun, M.: “Aerodynamics and aeroelasticity of a HP compressor during surge and reversed flow”, Proceedings of the 12<sup>th</sup> ISUAAAT, Sept. 1-4, 2009, London, UK
- [18] Cinnella, P.; De Palma, P.; Pascazio, G.; Napolitano, m.: “A Numerical Method for Turbomachinery Aeroelasticity”, J. Turbomach. Volume 126, Issue 2, 310-316
- [19] Rottmeier F., “Experimental investigation of a vibrating axial turbine cascade in presence of upstream generated aerodynamic gusts”, Thèse EPFL no. 2758, 2003, Lausanne